Optimal sensing of photon addition or subtraction from quantized light

S. Lakshmi Bala
Centre for Quantum Information, Communication and Computing (CQuICC), IIT Madras,
Chennai, India

References: (1) Optimal sensing of photon addition and subtraction on nonclassical light, Soumyabrata Paul, Arman, S. Lakshmibala, Prasanta Panigrahi, S. Ramanan and V. Balakrishnan Phys.Rev.A, 111(4) April 2025; DOI: 10.1103/PhysRevA 111, L040601

This paper addresses the several advantages of working with tomograms (avoiding state reconstruction), and the usefulness of the Wasserstein distance in the context of addition and subtraction of photons to nonclassical light such as the single mode squeezed vacuum, the even cat state and the odd cat state.

(2) Efficacy of tomographic markers and photon addition to coherent states of light: Comparison with experiment, Soumyabrata Paul, S. Lakshmibala, V. Balakrishnan and S. Ramanan, Arxiv quant.phys. arxiv:2401:16098 (submitted to Optics Letters)

This paper addresses the advantageous of working with any of three tomographic markers of photon addition to quantized light These markers are the Wasserstein distance, the Kullback-Leibler divergence and the Bhattacharyya distance.

Comparison with a recently published experiment on photon addition to coherent light establishes the advantages of working with the tomographic approach and how these markers are successful.

The experimental paper with which comparisons are made is Experimental preparation of multiphoton-added coherent states of light, J. Fadrny, M.Neset, M.Bielak, M. Jezek, J.BÃlek, J. Fiurasek, npj Quantum Inf. 10, 89 (2024).

A partial small set of references

- An introduction to the tomographic picture of quantum mechanics, A Ibort, V I Man′ko, G Marmo, A Simoni and F Ventriglia Physica Scripta, Volume 79, 065103 (2009), DOI:10.1088/0031-8949/79/06/065013.
- Optical tomography of photon-added coherent states, even and odd coherent states and thermal states, Ya. A. Korennoy and V. I. Man′ko, 83, 053817 (2011); DOI: 10.1103 /PhysRevA.83.053817.
- Single-photon added coherent states:estimation of parameters and fidelity of the optical homodyne detection, S N Filippov, V I Man′ko, A S Coelho, A Zavatta, M Bellini, Physica Scripta, T153, 014025 (2013); DOI: 10.1088/0031-8949/2013/t153/014025.

- Tomograms are useful in several disciplines ranging from medical imaging to physics. A tomogram is essentially a 'scan'.
- At different 'angles' an output 'image' of an 'object' is obtained. Each 'image' therefore is a 'slice' of the full 'tomogram'. Each slice therefore carries partial information about the object
- The full 'object' is to be reconstructed from the tomogram (the set of all slices). In principle, this is an infinite number of slices.

Two major challenges.

- What is the optimal number of slices needed to reconstruct the 'object'? (Quantum state reconstruction). The number of slices needed depends on the system considered.
- Can we avoid detailed reconstruction of the 'object' and infer its properties from a finite set of slices of the tomogram (I.e., take a tomographic approach).

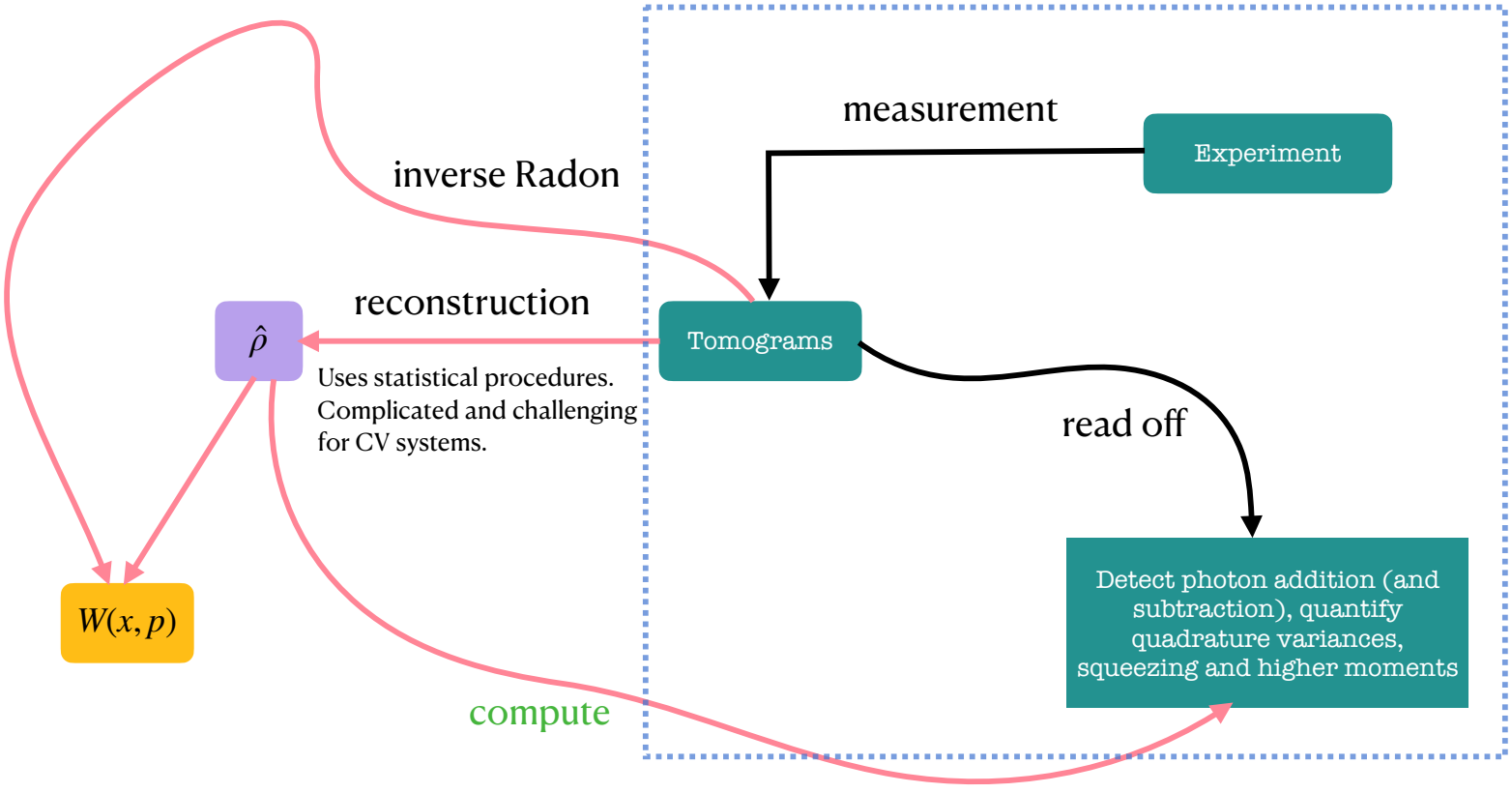

Flow chart for a quantum state reconstruction (QST) program. Highlighted is our approach which circumvents QST in the context of photon addition.

The single-mode optical tomogram (pure states): Tomogram obtained from multiple measurements of a set of observables which give complete information about the state (quorum). Rotated quadrature operators, $\mathbb{X}_\theta = \frac{1}{\sqrt{2}}(a^\dagger e^{i\theta} + a\, e^{-i\theta})$, Tomogram

$$\omega(X_\theta, \theta) = \langle X_\theta, \theta |\, \rho\, | X_\theta, \theta \rangle = |\, \langle X_\theta, \theta | \psi \rangle\, |^2.$$

$|X_\theta, \theta\rangle$: eigenvector of $\hat{X}_\theta$, with eigenvalue X_θ ($0 \leq \theta \leq \pi$). $X : \theta = 0$, $P : \theta = \pi/2$. We have a complete basis $|X_\theta\rangle$ for a fixed θ.
Note: $|X_\theta, \theta\rangle = e^{i\theta a^\dagger a}\, |X\rangle$.

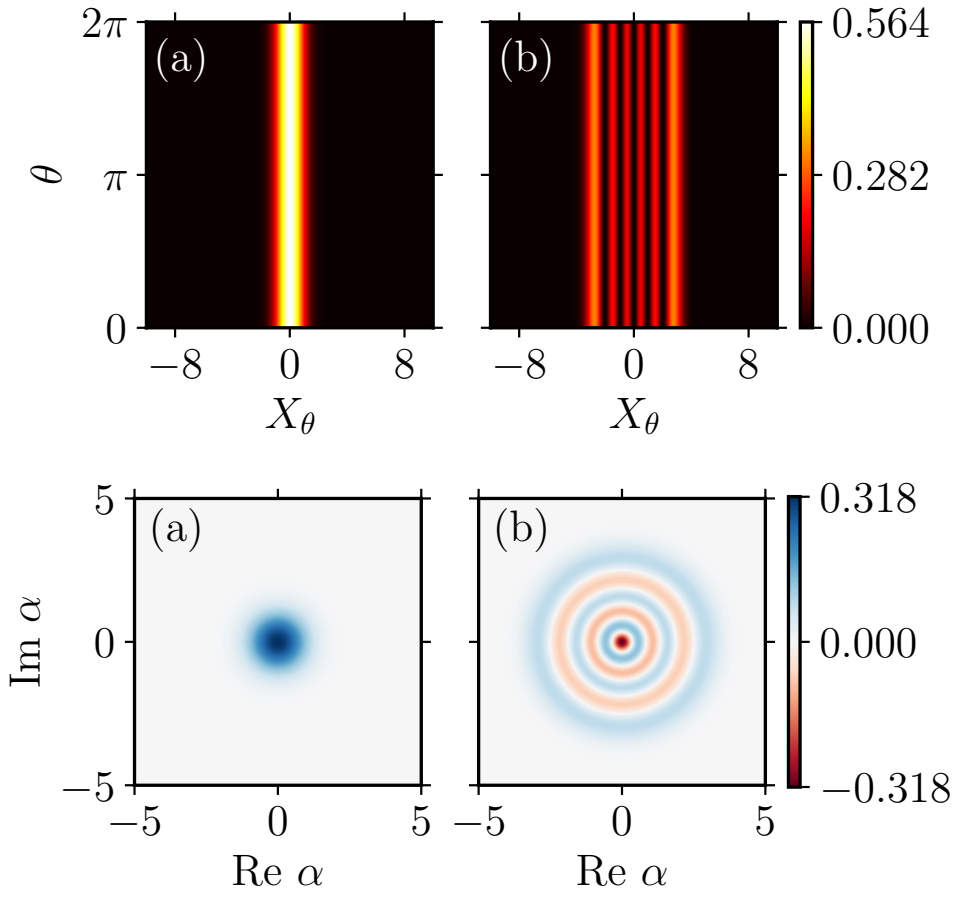

Top:Before state reconstruction Optical tomograms $\boldsymbol{w(X_\theta, \theta)}$ corresponding to (a) the **0**-photon state and (b) the **5**-photon state. In general, for the $\boldsymbol{n}$-photon state the tomogram has $\boldsymbol{n}$ vertical dark cuts. Bottom: After state reconstruction Wigner functions corresponding to (a) the **0**-photon state and (b) the **5**-photon state. Here $\mathbf{Re}\ \boldsymbol{\alpha = x/\sqrt{2}}$ and $\mathbf{Im}\ \boldsymbol{\alpha = p/\sqrt{2}}$.

States of light
Ex: Coherent light (CS)

$$|\alpha\rangle = e^{|\alpha|^2/2} \sum_p \frac{\alpha^p}{\sqrt{p!}} |p\rangle .$$

Here $|p\rangle$: p-photon state, α: complex number and $a|\alpha\rangle = \alpha|\alpha\rangle$.
m-photon added CS $|\alpha, m\rangle$ by repeated application of $a^\dagger$ (m times) on $|\alpha\rangle$, and normalizimg the state.
Squeezed vacuum (SSV) obtained by applying the squeezing operator on the zero photon state
Photon added and subtracted counterparts of SSV.
Field quadrature operators $X = \frac{a+a^\dagger}{\sqrt{2}}$ and $P = \frac{a-a^\dagger}{\sqrt{2}i}$.

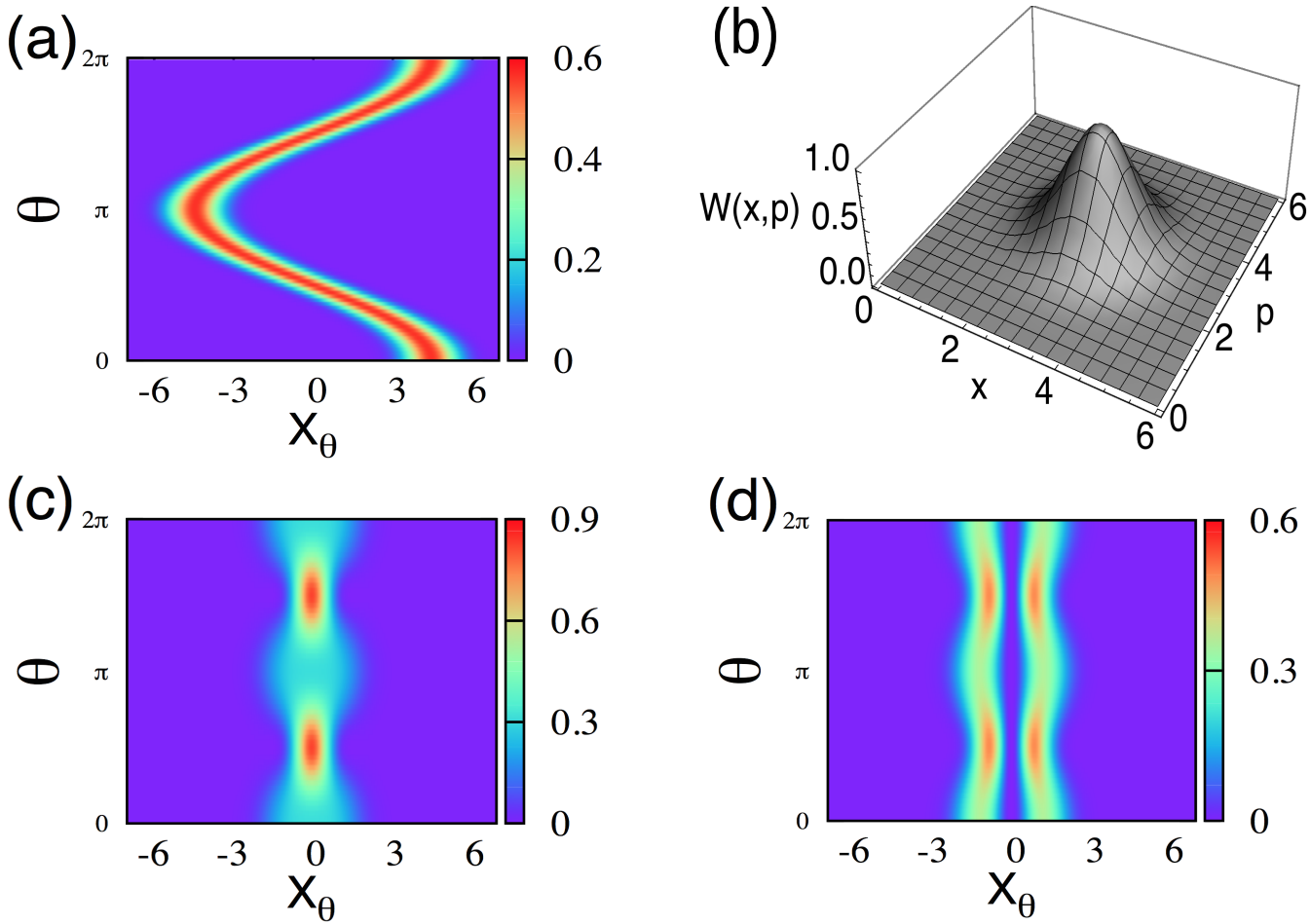

(a) The optical tomogram and (b) the Wigner function of the CS. (c) Optical tomogram of ECS $(|\alpha\rangle + |-\alpha\rangle)$ and (d) OCS $(|\alpha\rangle - |-\alpha\rangle)$ with $|\alpha|^2 = \mathbf{0.5}$.

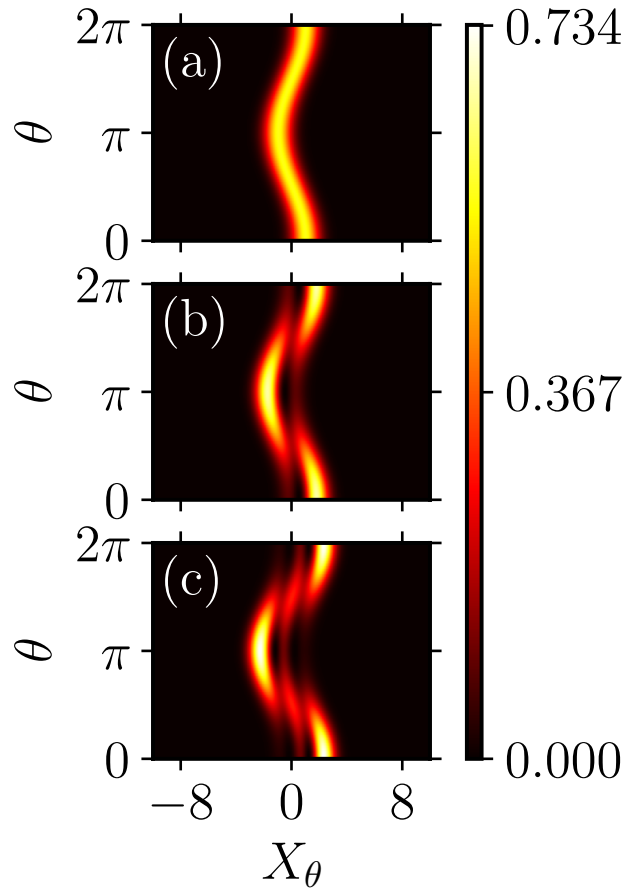

Optical tomograms corresponding to (a) $|\boldsymbol{\alpha}\rangle$, (b) $|\boldsymbol{\alpha}, \mathbf{1}\rangle$ and (c) $|\boldsymbol{\alpha}, \mathbf{2}\rangle$ for $\boldsymbol{\alpha} = \mathbf{0.7}$. Note that the tomogram for $|\boldsymbol{\alpha}, \mathbf{1}\rangle$ has one vertical cut, and that for $|\boldsymbol{\alpha}, \mathbf{2}\rangle$ has two vertical cuts. In general, it can be seen that the tomogram for $|\boldsymbol{\alpha}, \boldsymbol{m}\rangle$ has $\boldsymbol{m}$ vertical cuts.

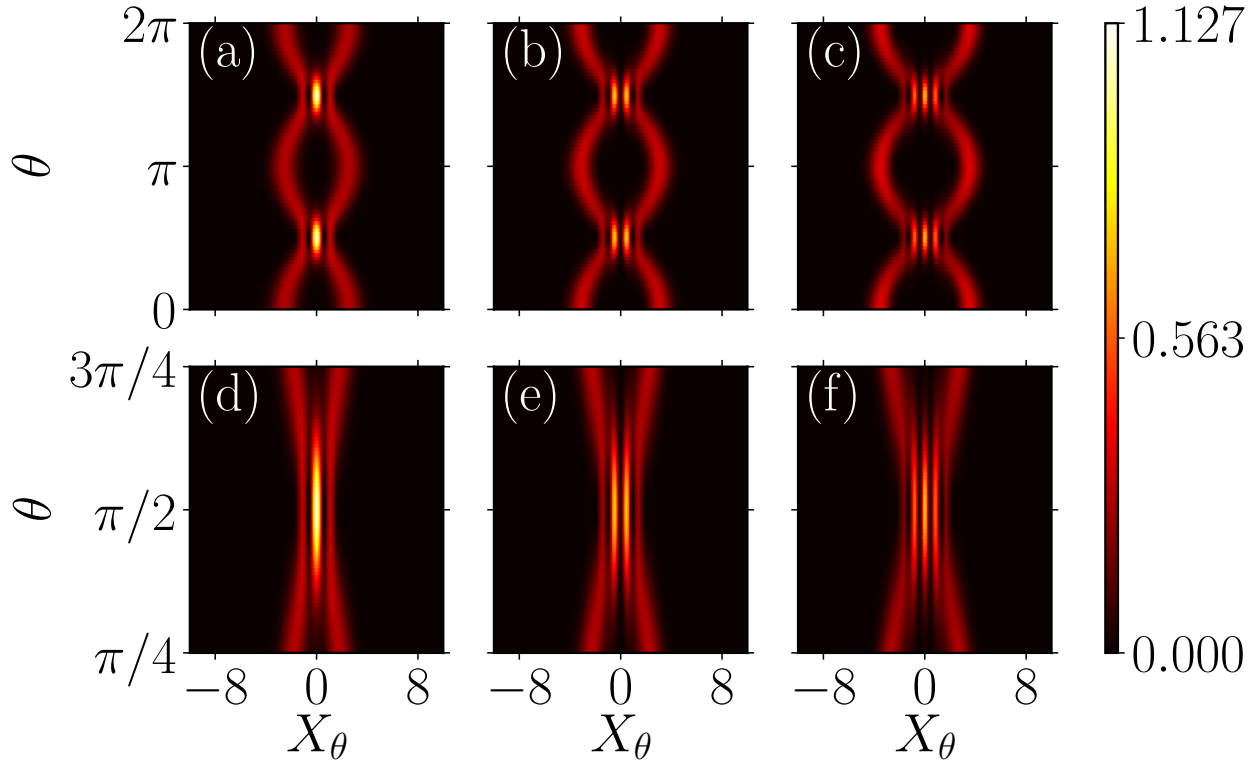

Top panel: Left to right: Single-mode optical to- mograms for (a) the ECS $|\alpha_+\rangle$, and its photon added counterparts (b) $|\alpha_+, \mathbf{1}\rangle$, and (c) $|\alpha_+, \mathbf{2}\rangle$. We set $\alpha = \mathbf{1.8}$, so that $|\alpha\rangle$ and $|-\alpha\rangle$ (comprising the ECS) are sufficiently apart, for the interference fringes to be clearly visible. Notice that intensity shifts are seen at $\theta = \pi/2$ and $3\pi/2$, with addition of photons.

Bottom panel: Left to right: Zoomed in versions.

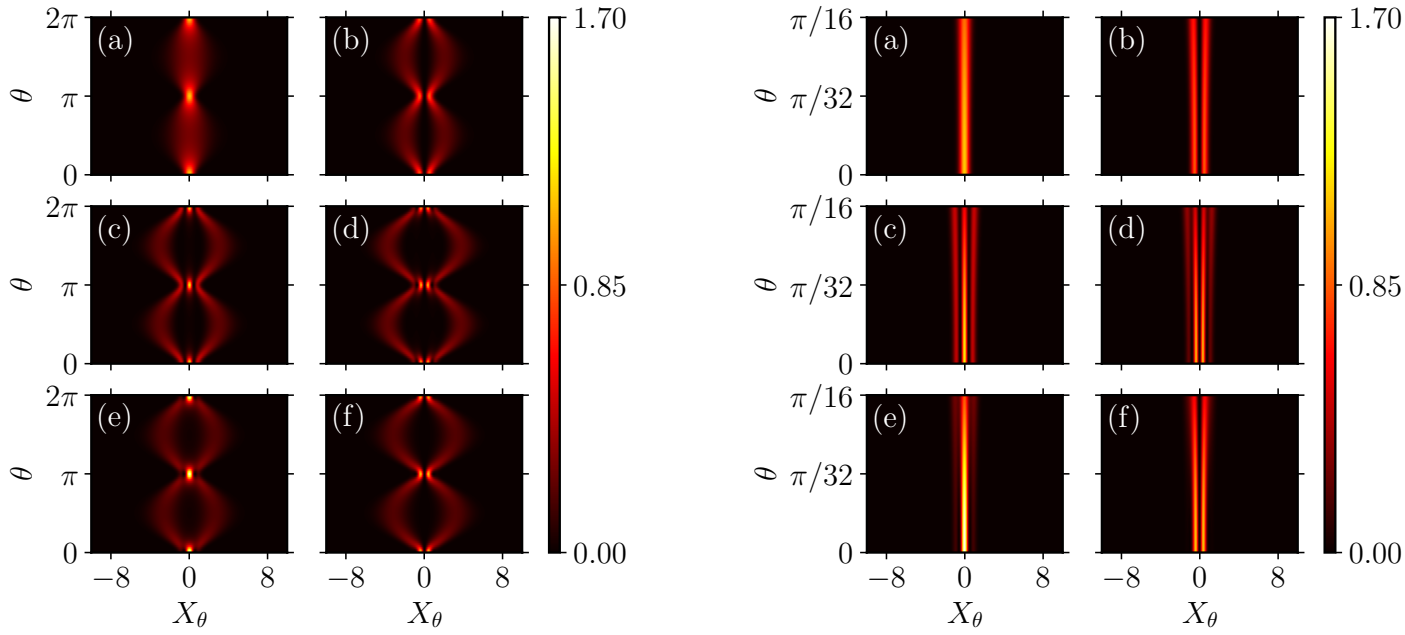

Left: Optical tomograms corresponding to the (a) SVS $|\boldsymbol{\xi}\rangle$, (b) $|\boldsymbol{\xi}, \mathbf{1}\rangle$ (or $|\boldsymbol{\xi}, -\mathbf{1}\rangle$), (c) $|\boldsymbol{\xi}, \mathbf{2}\rangle$, (d) $|\boldsymbol{\xi}, \mathbf{3}\rangle$, (e) $|\boldsymbol{\xi}, -\mathbf{2}\rangle$, and (f) $|\boldsymbol{\xi}, -\mathbf{3}\rangle$. The shift in the tomographic intensity pattern (at $\boldsymbol{\theta = 0}$, $\boldsymbol{\pi}$, $\boldsymbol{2\pi}$ of the SVS $|\boldsymbol{\xi}\rangle$ with addition or subtraction of photons is seen. There are striking similarities between tomograms corresponding to states which are superpositions of even photon no. states (equivalently, for states which are superpositions of odd photon no.states) particularly in the intensity of the central bright (equivalently dark) fringe.

Right: Corresponding zoomed-in versions close to $\boldsymbol{\theta = 0}$.

The bright central region at $\boldsymbol{\theta = 0}$, $\boldsymbol{\pi}$, $\boldsymbol{2\pi}$ in (a) indicates a peak in the PDF.
Addition or subtraction of a single photon to the SVS $|\boldsymbol{\xi}\rangle$ destroys this peak (the central dark region in (b)).
With the addition or subtraction of two photons the bright central region reappears ((c) and (e)).
With the addition or subtraction of three photons the bright central region disappears, and is replaced by a central dark region ((d) and (f)).

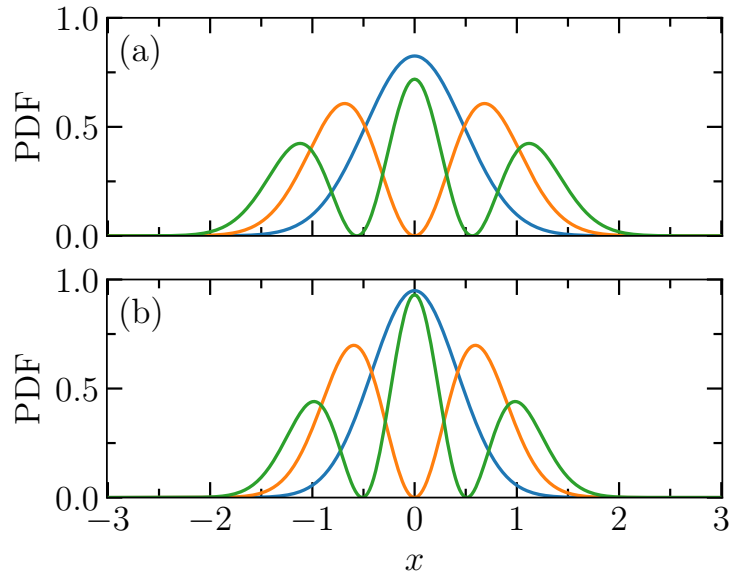

Probability distribution function (PDF) along $\boldsymbol{x}$-quadrature for $|\boldsymbol{\xi}\rangle$ (blue), $|\boldsymbol{\xi}, \mathbf{1}\rangle$ (orange), and $|\boldsymbol{\xi}, \mathbf{2}\rangle$ (green) for $\boldsymbol{r} =$ (a) $\mathbf{0.38}$ and (b) $\mathbf{0.52}$.

At $\boldsymbol{x} = \mathbf{0}$, the PDF for the SVS $|\boldsymbol{\xi}\rangle$ and the two-photon added SVS $|\boldsymbol{\xi}, \mathbf{2}\rangle$ are maximum, while the one-photon added SVS $|\boldsymbol{\xi}, \mathbf{1}\rangle$ has a corresponding minimum. This is reflected in the shift in the intensity patterns seen in the tomograms.

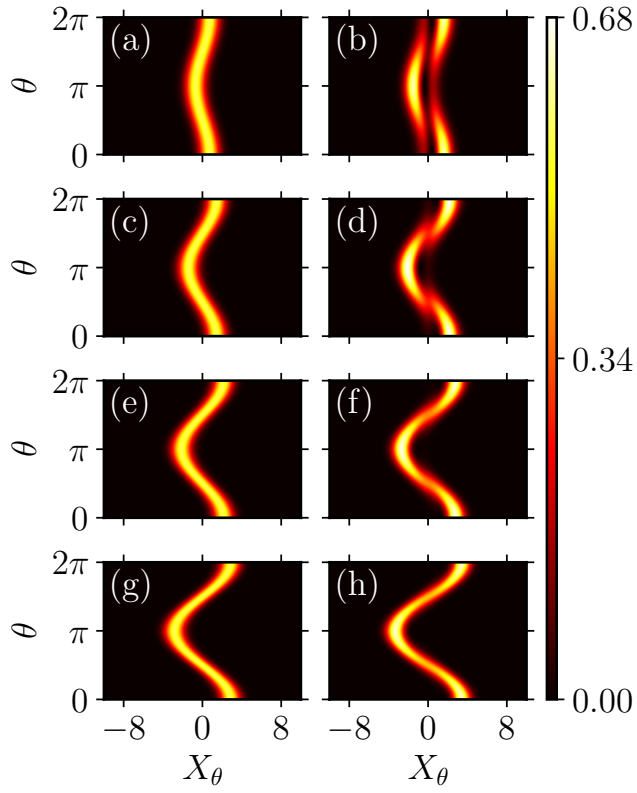

Left column panels : CS $|\mathbf{g_1(\alpha)\alpha}\rangle$, and Right column panels: $|\boldsymbol{\alpha}, \mathbf{1}\rangle$. $\boldsymbol{\alpha} = \mathbf{0.5}$ for (a) and (b), $\mathbf{1.0}$ for (c) and (d), $\mathbf{1.5}$ for (e) and (f), and $\mathbf{2.0}$ for (g) and (h) . For $|\boldsymbol{\alpha}| > \mathbf{1}$, the vertical cut in the tomograms corresponding to $|\boldsymbol{\alpha}, \mathbf{1}\rangle$ is absent, making them visually appear like the tomogram for the coherent state [see ,for example, (e) – (h)].

- Classical and quantum amplification

  Hence for $|\alpha| > 1$ the fidelity between $|g_1(\alpha)\alpha\rangle$ and $|\alpha, 1\rangle$ is maximized (experiment reported by J. Fadrný *et al.* npj Quantum Inf. **10**, 89 (2024)).

  $g_m(\alpha)\alpha$ is the amplification gain. The fidelity between a CS $|g_m(\alpha)\alpha\rangle$ and $|\alpha, 1\rangle$, can be easiliy shown to be maximized if

  $g_m(\alpha) = (\langle \alpha, m|a|\alpha, m\rangle)/|\alpha|$.

  We have computed $g_m(\alpha)$ directly from the tomograms for each α and shown that these plots of $g_m(\alpha)$ versus α $(m = 1, 2)$ reproduce the experimental plots obtained after state reconstruction $(m = 1, 2)$.

Procedure: From the tomogram, the following expectation values can be computed.

$$\langle \hat{a}^{\dagger k} \hat{a}^{l} \rangle = C_{kl} \sum_{m=0}^{k+l} \exp\left\{ -\frac{im(k-l)\pi}{k+l+1} \right\} \times \int_{-\infty}^{\infty} dX_\theta \; w\left(X_\theta, \frac{m\pi}{k+l+1}\right) H_{k+l}(X_\theta), \qquad (1)$$

where $C_{kl} = k!l!/\{(k+l+1)!2^{(k+l)/2}\}$ and $H_{k+l}(X_\theta)$ is the Hermite polynomial of degree $k+l$ computed as a function of X_θ for a given θ. Since $\theta = (m\pi)/(k+l+1)$ in the above expression, it is clear that $(k+l+1)$ slices of the tomogram including $\theta = 0$ are needed to compute $\langle \hat{a}^{\dagger k} \hat{a}^{l} \rangle$. Ref: "Tomographic reconstruction of the density operator from its normally ordered moments" by A. Wünsche, Phys. Rev. A **54**, 5291 (1996).
Set $k = 0$, $l = 1$ to compute $g_m(\alpha) = (\langle \alpha, m|a|\alpha, m\rangle)/|\alpha|$.

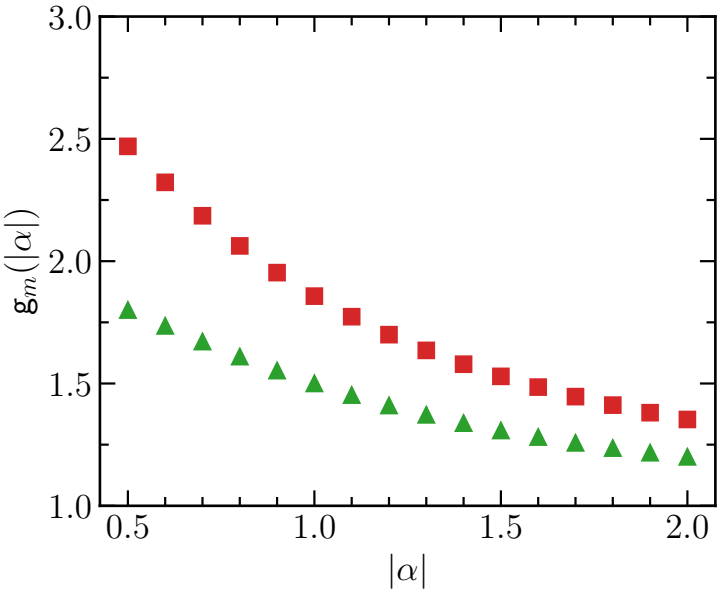

The above are our plots of the amplification gain $\mathbf{g_m(|\alpha|) = \langle \alpha, m|a|\alpha, m\rangle/|\alpha|}$ due to addition of photons, as functions of $|\alpha|$ for $\boldsymbol{m = 1}$ (green triangles) and 2 (red squares) respectively, computed from the tomograms.

In the experiment, $\mathbf{g_m(|\alpha|)}$ has been explicitly computed from the reconstructed state $|\alpha, m\rangle$.

Also used the theoretical expression for $|\alpha, m\rangle$, and calculated the amplification gain. These are identical to our plots.

The experimental data for the range of values of $|\alpha|$ considered ($\mathbf{0.5 \leqslant |\alpha| \leqslant 2}$), and these computations show that $\mathbf{g_m(|\alpha|)}$ is a decreasing function of $|\alpha|$.

Although the tomograms for $|\mathbf{g}_{m}(|\alpha|)\alpha\rangle$ and $|\alpha, m\rangle$ are visually similar, the variances say, along the x-quadrature computed directly from these tomograms are different.
Accurate computation of the mean, and all higher moments of the quadrature variables (in any quadrature) can be carried out directly from the tomogram.
For instance, if we choose the x-quadrature, the tomogram gives us the numerical value of $|\psi(x)|^2$ which can be read off at every x.
$\int_{-\infty}^{\infty} dx x^n |\psi(x)|^2$ can now be computed (treating the integration as a summation) to get the nth moment of x. Similar computations can be done in other quadratures.

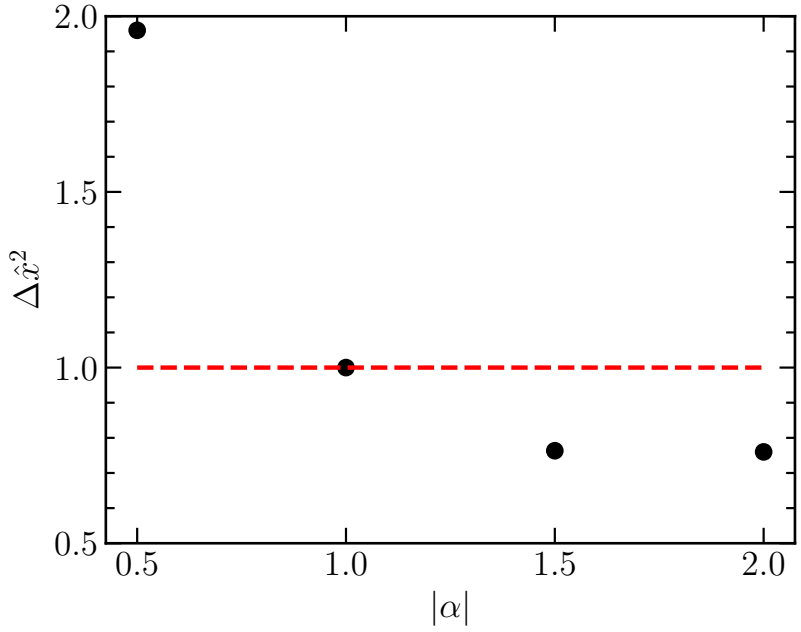

$\boldsymbol{\Delta\hat{x}^2}$ (black circles) corresponding to $|\boldsymbol{\alpha, 1}\rangle$, computed directly from the tomograms for $|\boldsymbol{\alpha}| = \boldsymbol{0.5, 1.0, 1.5}$ and $\boldsymbol{2.0}$.
Horizontal red line: Variance for the CS $|\mathbf{g_1}(\boldsymbol{\alpha})\boldsymbol{\alpha}\rangle$ computed directly from the tomograms for different values of $\boldsymbol{\alpha}$. Independent of $\boldsymbol{\alpha}$, as expected. Set to unity for ready comparison with the experiment. For $|\boldsymbol{\alpha}| = \boldsymbol{1}$, $\boldsymbol{\Delta\hat{x}^2}$ for both $|\mathbf{g_1}(\boldsymbol{\alpha})\boldsymbol{\alpha}\rangle$ and $|\boldsymbol{\alpha, 1}\rangle$ are equal. For $|\boldsymbol{\alpha}| > \boldsymbol{1}$, $\boldsymbol{\Delta\hat{x}^2} < \boldsymbol{1}$ for $|\boldsymbol{\alpha, 1}\rangle$ indicating that $|\boldsymbol{\alpha, 1}\rangle$ is squeezed along $\boldsymbol{x}$ Thus, amplified CS does not display squeezing but photon addition to the coherent state shows quantum amplification. At $\boldsymbol{\alpha = 1}$, the $\boldsymbol{p}$ quadrature variance will be different for both these states.

Tomographic markers (directly computable from the tomogram, to obtain the 'distance' between two probability density functions (PDFs). (Important in photon addition and subtraction to a reference state such as CS, SSV, ECS etc.)
Consider two normalized PDFs $f(x)$ and $g(x)$, with corresponding cumulative distribution functions (CDFs) $F(x) = \int_{-\infty}^{x} dy\ f(y)$ and $G(x) = \int_{-\infty}^{x} dy\ g(y)$. The Wasserstein distance (more accurately, the **1**-Wasserstein distance) between $F(x)$ and $G(x)$ is given by

$$W_1(F, G) = \int_{-\infty}^{\infty} dx\, |F(x) - G(x)|\,. \tag{2}$$

$W_1(F, G)$ is the optimal cost of reshaping $f(x)$ into $g(x)$, the cost being defined as the integrated probability mass shifted times the distance. (Earth mover's distance). W_1 is basis dependent.

Apart from W_1, we can use the Kullback-Leibler divergence D_{KL} or the Bhattacharyya distance D_B.

$$D_{\mathrm{KL}}(f,g) = \int_{-\infty}^{\infty} dx\, f(x) \ln [f(x)/g(x)], \tag{3}$$

$$D_{\mathrm{B}}(f,g) = -\ln \int_{-\infty}^{\infty} dx\, [f(x)g(x)]^{1/2}. \tag{4}$$

(Unlike W_1, D_{KL} and D_{B} are not proper distance functions in the space of distributions.) Modifications of D_{KL} : Example is the cumulative residual divergence (CRKL). Here, the PDFs $f(x)$ and $g(x)$ are replaced by $\widetilde{f}(x)$ and $\widetilde{g}(x)$, where $\widetilde{f}(x) = S(x)/\int_{-\infty}^{\infty} S(y)dy$ (and similarly for $\widetilde{g}(x)$), $S(x) = 1 - F(x) = \int_x^{\infty} S(y)dy$ being the survival function corresponding to $f(x)$. CRKL does not, in general, distinguish between probability distributions as markedly as D_{KL} itself. Furthermore, both $W_1$and D_{KL} are more readily applicable in machine learning protocols.

Two main comparisons with the experiment on photon addition to the CS.

- Expt: Fidelities between $|\mathbf{g_m(\alpha)}\alpha\rangle$ and $|\alpha, \boldsymbol{m}\rangle$, versus $|\alpha|$. (Classical and Quantum amplification).
- Expt: Fidelities between $|\boldsymbol{\beta_{opt}}\rangle$ and $|\alpha, \boldsymbol{m}\rangle$, versus $|\alpha|$. $|\boldsymbol{\beta_{opt}}\rangle$ is the CS of optimal amplitude with which $|\alpha, \boldsymbol{m}\rangle$ has the maximum fidelity.
  $\beta_{\mathrm{opt}} = |\alpha|[\mathbf{1} + (\mathbf{1} + \mathbf{4}\boldsymbol{m}/|\alpha|^{\mathbf{2}})^{\mathbf{1/2}}]/\mathbf{2}$,.
- If fidelities increase with $|\alpha|$, $\boldsymbol{W_1}$, $\boldsymbol{D_{KL}}$ and $\boldsymbol{D_B}$ should decrease, following similar trends. Also if fidelity increases asymptotically to its maximum value of 1, these markers must asymptotically decrease to 0.

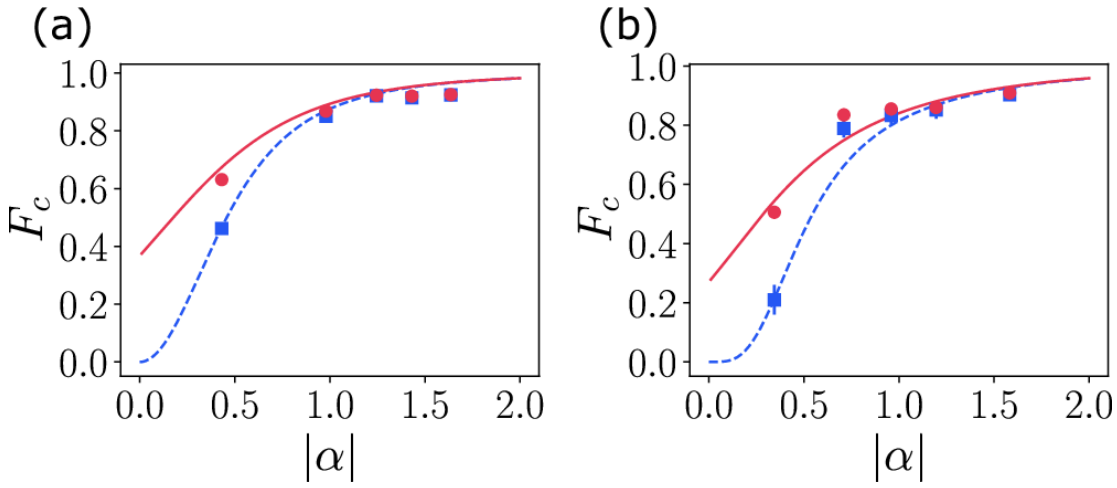

Plots from expt.: Fidelities of $|\alpha, m\rangle$ (obtained after state reconstruction) with the CS $|g_m(\alpha)\alpha\rangle$ and with the CS $|\beta_{opt}\rangle$ versus $|\alpha|$.

Theoretical computation of fidelity between reconstructed $|\alpha, m\rangle$ and $|\beta_{opt}\rangle$ are red solid lines, and between reconstructed $|\alpha, m\rangle$ and $|g_m(\alpha)\alpha\rangle$ are blue dashed lines. (a): $m = 1$, and (b) $m = 2$.

These figures are taken from the paper by Fadrny et.al., npj Quantum Information **10** 89 (2024).

Note: Fidelity with $|\beta_{opt}\rangle$ is higher for small $|\alpha|$. Beyond $\alpha = 1$ both fidelities match.

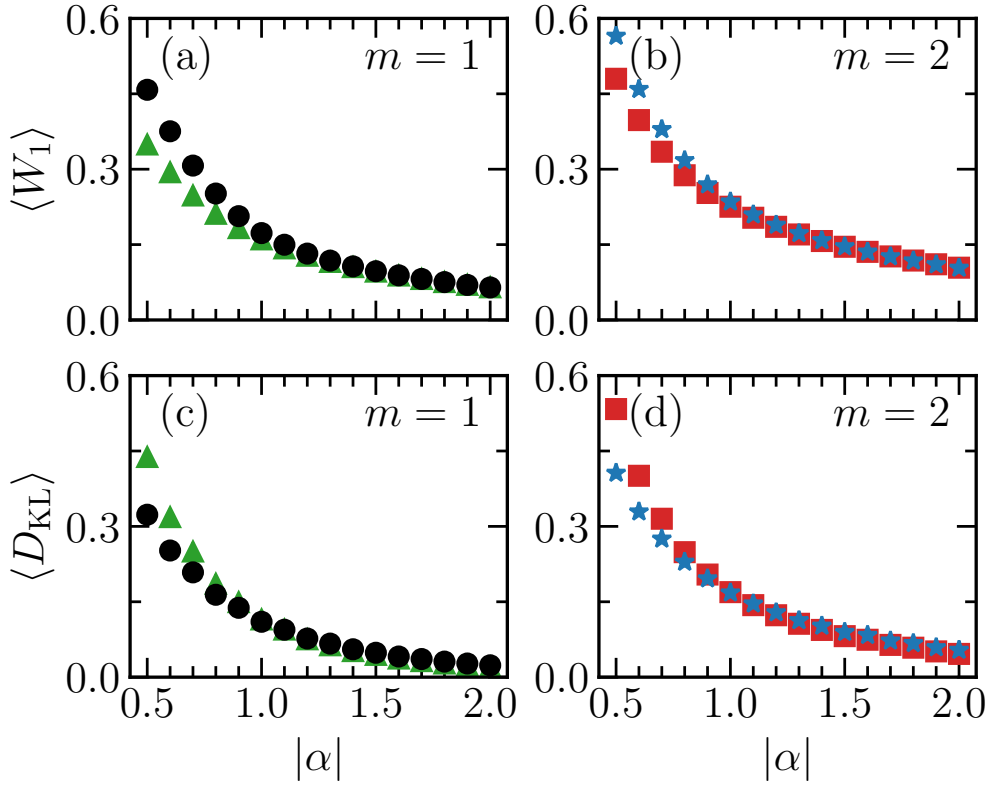

Average over **5** tomographic slices, i.e., **5** values of θ equally spaced between **0** and π. This suffices. Trends are good.
Top panel: $\langle \boldsymbol{W_1} \rangle$ between $|\boldsymbol{\alpha, m}\rangle$ and $|\boldsymbol{g_m(\alpha)\alpha}\rangle$ ($\boldsymbol{m = 1}$:green triangles and $\boldsymbol{m = 2}$: red squares), and between $|\boldsymbol{\alpha, m}\rangle$ and $|\boldsymbol{\beta_{opt}}\rangle$ ($\boldsymbol{m = 1}$;: black circles and $\boldsymbol{m = 2}$ blue asterisks),
Bottom panel: $\boldsymbol{D_{kl}}$ between $|\boldsymbol{\alpha, m}\rangle$ and $|\boldsymbol{g_m(\alpha)\alpha}\rangle$ ($\boldsymbol{m = 1}$: green triangles and $\boldsymbol{m = 2}$: red squares), and between $|\boldsymbol{\alpha, m}\rangle$ and $|\boldsymbol{\beta_{opt}}\rangle$ ($\boldsymbol{m = 1}$: black circles and $\boldsymbol{m = 2}$: blue asterisks).

For small $|\alpha|$, the plots for D_{KL} are consistent with the experimental result (for a given m, D_{KL} between $|\alpha, m\rangle$ and $|\beta_{opt}\rangle$ is smaller than that between $|\alpha, m\rangle$ and $|g_m(\alpha)\alpha\rangle$. W_1 marginally departs from this as it is the transportation cost of transforming one PDF to another. For $m = 1$, in the case of $|\beta_{opt}\rangle$, W_1 tends to the distance between $|1\rangle$ and the CS $|\alpha = 1\rangle$, whereas in the case of $|g_m(\alpha)\alpha\rangle$, it tends to the corresponding distance between $|1\rangle$ and $|0\rangle$. The transportation distance between a Gaussian and a shifted Gaussian is responsible for the departure mentioned above. A similar argument holds for higher values of m.
($\beta_{\text{opt}} = |\alpha|[1 + (1 + 4m/|\alpha|^2)^{1/2}]/2$,)

Important feature: No crossovers. (W_1 does not have the same numerical value for both $m = 1$ and 2, for a given $|\alpha|$. W_1 increases with increase in m.

Similarly D_{KL} and D_B. Always D_B follows the same trends as D_{KL}.

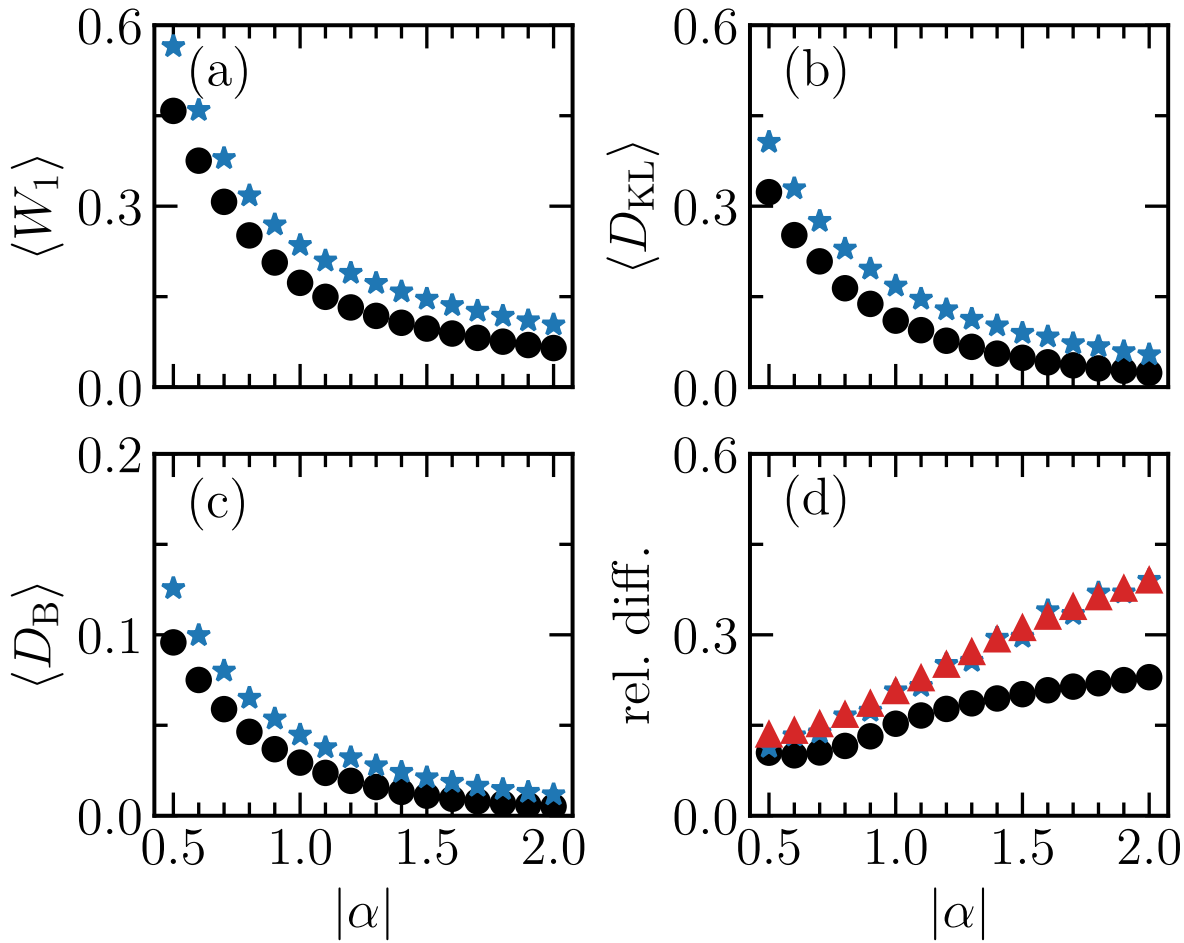

Moving on to photon addition to squeezed vacuum

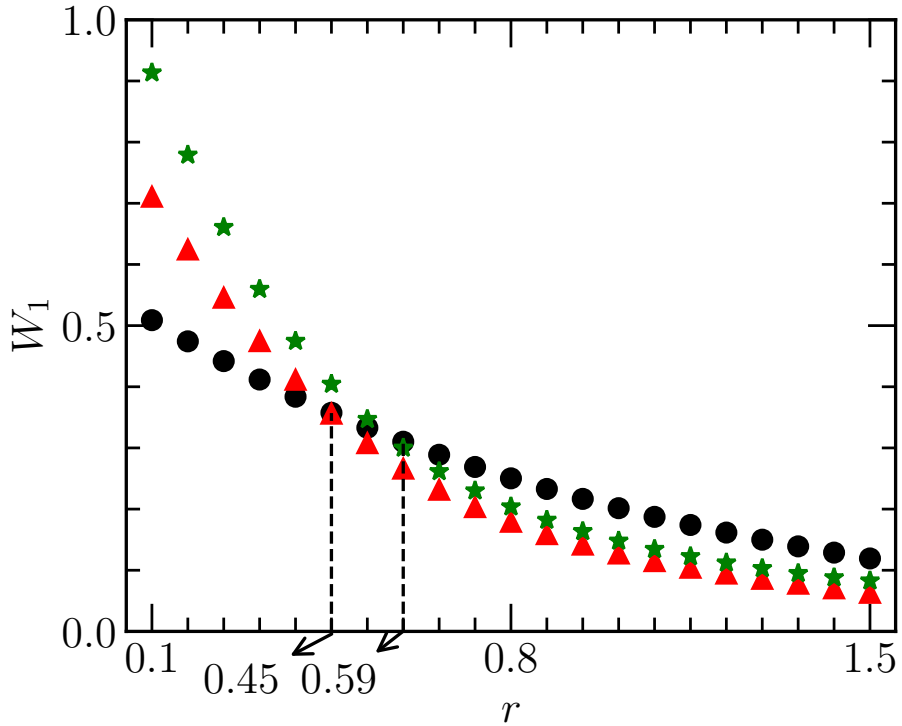

$\boldsymbol{W_1}$ between $|\xi\rangle$ and $|\xi, \mathbf{1}\rangle$ [or $|\xi, -\mathbf{1}\rangle$] (black circles), $|\xi\rangle$ and $|\xi, \mathbf{2}\rangle$ (red triangles), and $|\xi\rangle$ and $|\xi, \mathbf{3}\rangle$ (green asterisks) versus squeezing parameter $\boldsymbol{r}$, along $\boldsymbol{x}$-quadrature.
The crossovers between $\boldsymbol{W_1}$ for 1- photon and 2- photon addition is at $\boldsymbol{r}$ approx. **0.45** and between 1 and 3 photon addition is at $\boldsymbol{r}$ approx. **0.59**.
To distinguish between photon added counterparts using $\boldsymbol{W_1}$ avoid the neighborhood of values of $\boldsymbol{r}$ where crossovers occur.

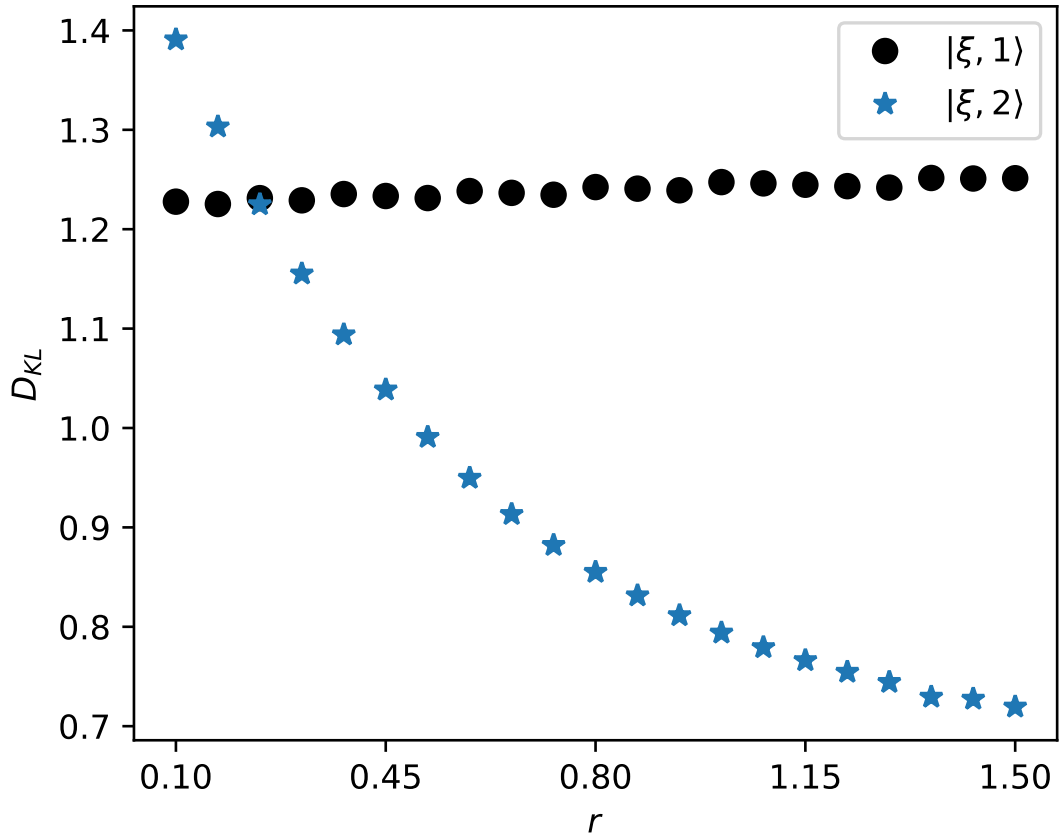

Ref. state is $|\xi\rangle$. $\boldsymbol{D_{KL}}$ between $|\xi\rangle$ and $|\xi, \mathbf{1}\rangle$ is not very sensitive to $\boldsymbol{r}$. Logarithmic dependence in $\boldsymbol{D_{KL}}$ not sensitive to $\boldsymbol{r}$, but crossover is seen at $\boldsymbol{r}$ approx. $\mathbf{0.3}$. $\boldsymbol{D_B}$ is sensitive to $\boldsymbol{r}$ like $\boldsymbol{W_1}$, even for 1 photon addition. $\boldsymbol{D_{KL}}$, $\boldsymbol{W_1}$ and $\boldsymbol{D_B}$. between $|\xi\rangle$ and $|\xi, \mathbf{2}\rangle$ are all sensitive to $\boldsymbol{r}$. Crossovers seen in all cases.

Summary and outlook

- Addition of photons to the CS, and addition and subtraction of photons to the SVS and ECS investigated directly from tomograms, circumventing state reconstruction.
- Visual inspection of the tomograms plus computation of quadrature variances in canonically conjugate quadratures (if necessary) directly from tomograms, augmented with mean photon number calculations(if necessary) directly from tomograms, suffices to identify the extent of photon addition or subtraction.
- Tomographic markers play an important role. Their variation with the relevant parameter $|\alpha|$ or the squeezing parameter etc., can be compared directly with experimentally obtained corresponding fidelity plots.

- Crossover phenomenon seen in the case of nonclassical light such as SVS and ECS, in certain quadratures.
- The Wasserstein distance, the Bhattacharyya distance and the Kullback-Leibler divergence are useful tomographic markers in this context.
- In single-mode light state reconstruction from tomogram is reasonably easy. Difficult for multimode states and hybrid systems. (Machine learning algorithms are employed in current literature). Extension of our procedure will be potentially very useful. (We have provided a proof of concept).